Systems-level immunomonitoring from acute to recovery phase of severe COVID-19

Lucie Rodriguez[1,8], Pirkka Pekkarinen[2,8], Tadepally Lakshmikanth[1,8], Ziyang Tan[1,8], Camila Rosat Consiglio[1,8], Christian Pou[1], Yang Chen[1], Constantin Habimana Mugabo[1], Anh Nguyen Quoc[3], Kirsten Nowlan[3], Tomas Strandin[4], Lev Levanov[4], Jaromir Mikes[1], Jun Wang[1], Anu Kantele[5], Jussi Hepojoki[4], Olli Vapalahti[4], Santtu Heinonen[6], Eliisa Kekäläinen[3,6], Petter Brodin[1,7,8,9]

[1] Science for Life Laboratory, Department of Women's and Children's Health, Karolinska Institutet, Sweden.

[2] Division of Intensive Care Medicine, Department of Anesthesiology, Intensive Care and Pain Medicine, University of Helsinki and Helsinki University Hospital, Finland.

[3] Translational Immunology Research Program, University of Helsinki and Helsinki University Hospital, Finland.

[4] Department of Virology, University of Helsinki and Helsinki University Hospital, Helsinki, Finland.

[5] Inflammation Center, Division of Infectious Diseases, University of Helsinki and Helsinki University Hospital, Finland.

[6] New Children's Hospital, Pediatric Research Center, University of Helsinki and Helsinki University Hospital, Finland.

[7] Department of Pediatric Rheumatology, Karolinska University Hospital, Sweden.

[8] Equal contribution

[9] Lead contact

SUMMARY

The immune response to SARS-CoV2 is under intense investigation, but not fully understood att this moment. Severe disease is characterized by vigorous inflammatory responses in the lung, often with a sudden onset after 5-7 days of stable disease. Efforts to modulate this hyperinflammation and the associated acute respiratory distress syndrome, rely on the unraveling of the immune cell interactions and cytokines that drive such responses. Systems-level analyses are required to simultaneously capture all immune cell populations and the many protein mediators by which cells communicate. Since every patient analyzed will be captured at different stages of his or her infection, longitudinal monitoring of the immune response is critical. Here we report on a systems-level blood immunomonitoring study of 39 adult patients, hospitalized with severe COVID-19 and followed with up to 14 blood samples from acute to recovery phases of the disease. We describe an IFNγ – Eosinophil axis activated prior to lung hyperinflammation and changes in cell-cell coregulation during different stages of the disease. We also map an immune trajectory during recovery that is shared among patients with severe COVID-19.

HIGHLIGHTS

Systems-level immunomonitoring from acute to recovery in severe COVID-19

An IFNγ - Eosinophil axis involved in lung hyperinflammation

Cell-cell coregulation differ during four disease stages

Basophils and hyperinflammation modulate humoral responses

A shared trajectory of immunological recovery in severe COVID-19

INTRODUCTION

Since its emergence in December 2019 the Severe Acute Respiratory Syndrome-Corona Virus 2 (SARS-CoV2) causing the disease COVID-19 has infected millions of individuals and caused hundreds of thousands of deaths worldwide. The betacoronavirus has high degree of sequence homology with previous SARS-CoV and MERS coronaviruses and bind to the angiotensin-converting enzyme 2, ACE2-receptor to enter cells in the respiratory and intestinal epitelium (Lu et al., 2020).

Cells recognize the presence of the virus and its RNA via cytosolic and endosomal Pathogen recognition receptors, PRR and elicit antiviral response programs (Medzhitov and Janeway, 2002). The two main components of such antiviral programs involve the production of type I and III Interferons that induce downstream transcription of hundreds of interferon-stimulated genes that interfere with viral replication in the cell (Lazear et al., 2019). The second element of the antiviral response program is the secretion of chemokines that recruit specialized cells of the immune system to clear the virus. SARS-CoV-2, like other viruses, has evolved countermeasures to these defenses and in particular, the virus efficiently interferes with IFN-signaling and the induction of ISGs in SARS-CoV-2 infected cells (Blanco-Melo et al., n.d.). In contrast, pro-inflammatory cytokine and chemokine responses are induced normally and this imbalance between antiviral and pro-inflammatory responses is a key feature of COVID-19 (Vabret et al., 2020).

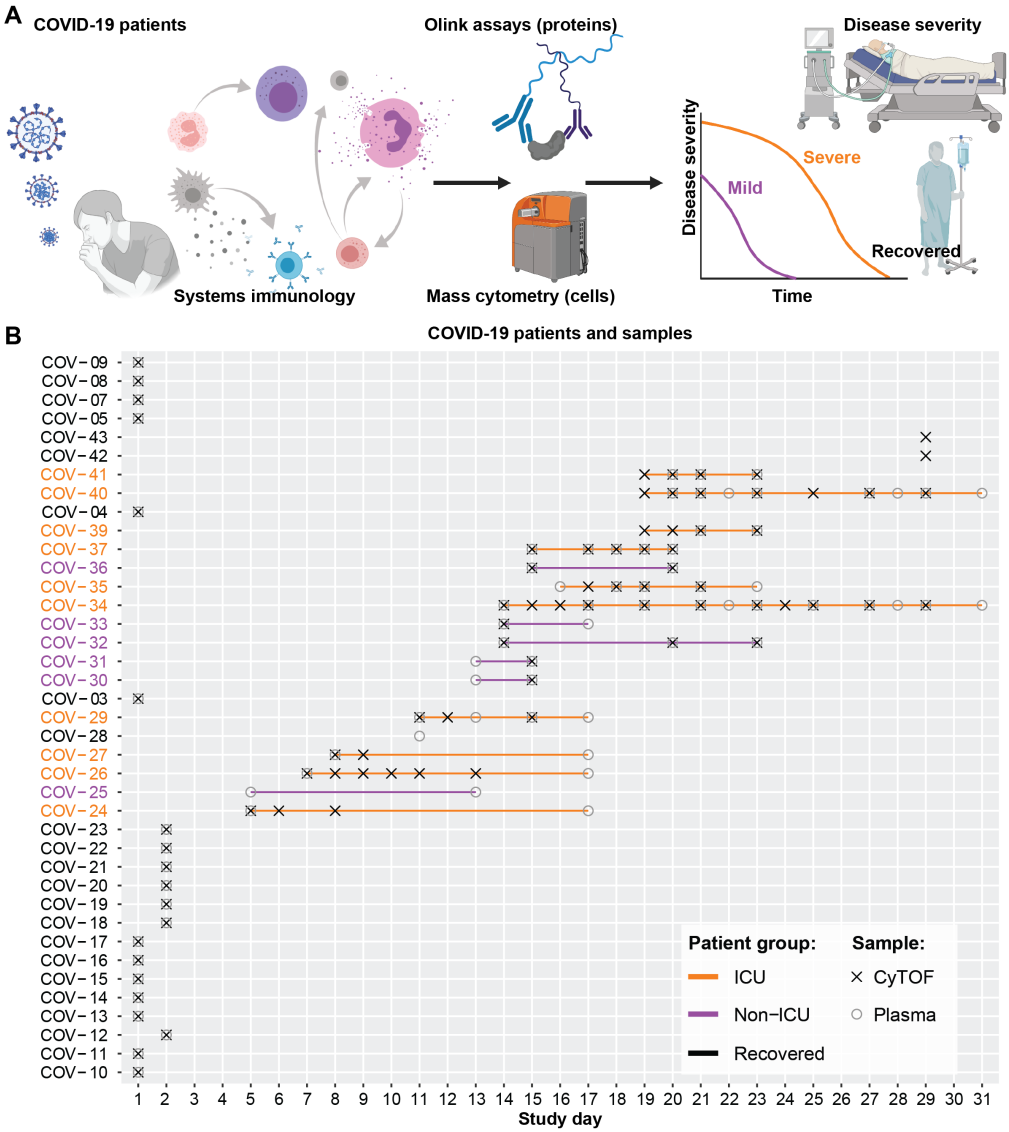

Figure 1. Lonitudinal profiling of the immune system in moderate and severe COVID-19. (**A**) 180 unique plasma proteins were quantiied using Olink assays (n=77 plasma samples) and whole blood immune cells analyzed by Mass cytometry (n=80 whole blood samples). (**B**) Monitoring and longitudinal sampling of blood cells (X) and plasma (o) from 39 patients at the University Hospital in Helsinki.

Another observation during the COVID-19 pandemic is the different disease courses among different individuals infected by SARS-CoV2 virus. Most individuals present with a very mild disease, often asymptomatic, and a few develop a life-threatening disease requiring intensive care. The strongest determinant of disease severity is age, with children presenting almost exclusively with mild disease (Brodin, 2020), while the elderly, over 70 years of age are much more likely to develop severe COVID-19. Males and females are

infected at similar rates, but males are much more likely to develop severe disease and requiring intensive care (Jin et al., 2020). Obesity, smoking and hypertension are other risk factors for severe COVID-19 (Huang et al., 2020). On the other hand, COVID-19 contrast with other respiratory viral infections in that pregnant women do not seem to be more likely to develop severe disease and this is also true for patients with various forms of immunodeficiency. One likely reason for these observations is that severe disease is associated with exuberant immune responses and a skewed immune regulation against pro-inflammatory responses in pregnancy and T-cell deficiencies in transplan patients make such hyperinflammatory responses less likely. To treat hyperinflammation in severe COVID-19 we need to better understand the cells involved, their interactions and

109 protein mediators used to orchestrate their response. To this end, we have
110 perfomed systems-level analyses of the immune system in blood from 39

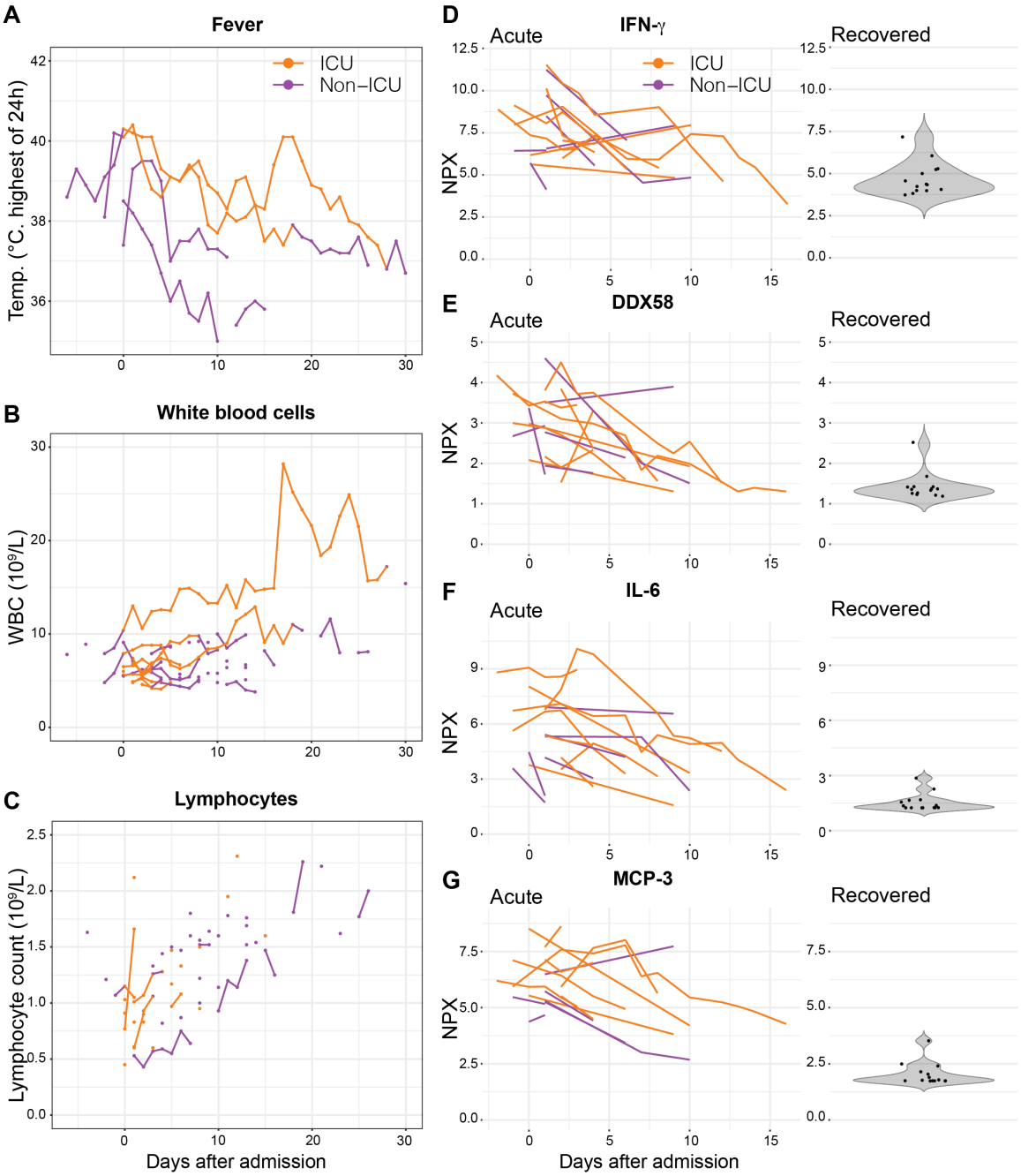

Figure 2. The natural course of severe COVID-19 from admission to clinical recovery. (**A**) Body temperature measurements from representative patients over the course of 30 days from admission to the hospital in ICU and non-ICU patients. (**B-C**) Whole blood cell counts, and Lymphocyte counts during acute and recovery phase in COVID-19 patients. (**D-G**) Plasma levels of the indicated proteins using Olink assays in longitudinal samples from acute patients (left) and single measurements from recovered patients (right). NPX: Normalized Protein expression.

111 patients, from acute to recovery phase of severe COVID-19, with up to 14 blood
112 samples collected from a given patient. These analyses reveal a sequence of
113 responses involving many immune cell populations at different stages of the
114 disease. A transient response involving IFNγ upregulating CD62L on Eosinophils
115 prior to lung hyperinflammation, examples of coregulated cell populations, and
116 immune correlates of productive antibody responses to SARS-CoV2 as well as
117 an integrated immune trajectory shared across patients recovering from severe
118 COVID-19.
119
120 **RESULTS**
121 **Longitudinal profiling of patients with COVID-19**
122 Given the enormous diversity among immune systems in humans, longitudinal
123 monitoring of patients is required to appreciate immunological changes occurring
124 during a disease process. Also, systems-level analyses methods such as Mass
125 cytometry (Brodin, 2018) enable all immune cell populations to be distinguished
126 and analyzed in a given blood sample, allowing for coordinated changes across
127 cell populations to be revealed. We have combined these cellular measurements
128 with analyses of 180 unique plasma proteins using Olink analyses (Lundberg et
129 al., 2011) (**Fig. 1a**). In order to understand systems-level immune responses
130 during moderate to severe COVID-19 we monitor longitudinal samples from 39
131 patients, some treated in the intensive care unit (ICU) and some treated in
132 regular hospital wards with oxygen support but no mechanical ventilation (**Fig.**
133 **1b**). Patients did not receive immunomodulatory therapies in this cohort and the
134 immunological changes reflect the natural course of the infection and all patients
135 survived the infection.
136
137 **The characteristics of acute and recovery phases of COVID-19**
138 Clinical measurements were taken from acute and recovered patients including
139 body temperature, white blood cell counts and lymphocyte counts. Milder cases
140 of COVID-19 showed lower body temperatures as well faster normalization of
141 body temperatures as compared to severe cases who fluctuated more over time

142 (**Fig. 2A**). The white blood cell (WBC) counts gave a possible correlate to the
143 stage of the infection. High WBC counts are often a reflection of acute
144 inflammation and immune responses and in severe patients we observed more
145 fluctuating levels of WBC over time (**Fig. 2B**). Also, there were no signs of
146 secondary bacterial infection in the patients in this cohort. Lymphopenia is one of
147 the common features of COVID-19 and the degree of lymphopenia predict
148 disease severity (Huang et al., 2020). Lymphocyte counts were measured and
149 found that milder cases recuperated their lymphopenia faster than severe cases
150 (**Fig. 2C**). This is in line with other previous reports (Lagunas-Rangel, 2020).
151 Plasma protein levels were observed and compared among acute and
152 recovered phases and map immune dynamics of severe COVID-19 (**Fig. 2D-G**).
153 Pro-inflammatory cytokines like IL-6 and IFNγ predict disease severity. A
154 decreasing trend is observed in IFNγ and IL-6 from early admission to the
155 hospital through recovery during the weeks of the study (**Fig. 2D and 2F,**
156 **respectively**). Similarly, DDX58, the Innate Immune Response Receptor also
157 called RIG-I, and the monocyte chemoattractant protein MCP-3, are elevated
158 during acute disease and decrease during recovery (**Fig. 2E and 2G,**
159 **respectively**).
160
161 **The immune cell changes from acute to recovery phase of COVID-19**
162 A defining feature of acute immune responses during COVID-19 is dramatic
163 changes in immune cell composition that can be informative of likely driving
164 factors and triggers. To understand severe COVID-19 better we plot relative
165 proportions of 57 immune cell populations over time in the 39 patients (**Fig. 3**).
166 We confirm the overrepresentation of Neutrophils over Lymphocytes during acute
167 infection, that is slowly reversed during the recovery phase (**Fig. 3**). This is in line
168 with reports suggesting the Neutrophil-to-Lymphocyte ratio (NLR) and degree of
169 lymphopenia are predictive of disease severeity in COVID-19 (Lagunas-Rangel,
170 2020). The plasmablast response is clear and occurs during the first week after
171 admission in these patients (**Fig. 3**). The recovery of T-cells after the initial
172 lymphopenia occurs over the following 2-3 weeks and is dominated by CD127

expressing effector and central memory CD4⁺ T-cells, as well as CD57-expressing and differentiated memory CD8⁺ T-cells (**Fig. 3**). Also, all Dendritic cell (DC) subsets increased from acute to recovery phases, CD1c⁺ DCs, CD11c⁺ DCs and plasmacytoid DCs (pDC) (**Fig. 3**). Also, despite a clear reduction in relative abundance of neutrophils over time, the other granulocyte subsets, Basophils and Eosinophils increased clearly from acute to recovery phases (**Fig. 3**), and both of these were among the most dynamic cell populations during severe disease, suggestive of important contributions to the antiviral defense and immunopathology.

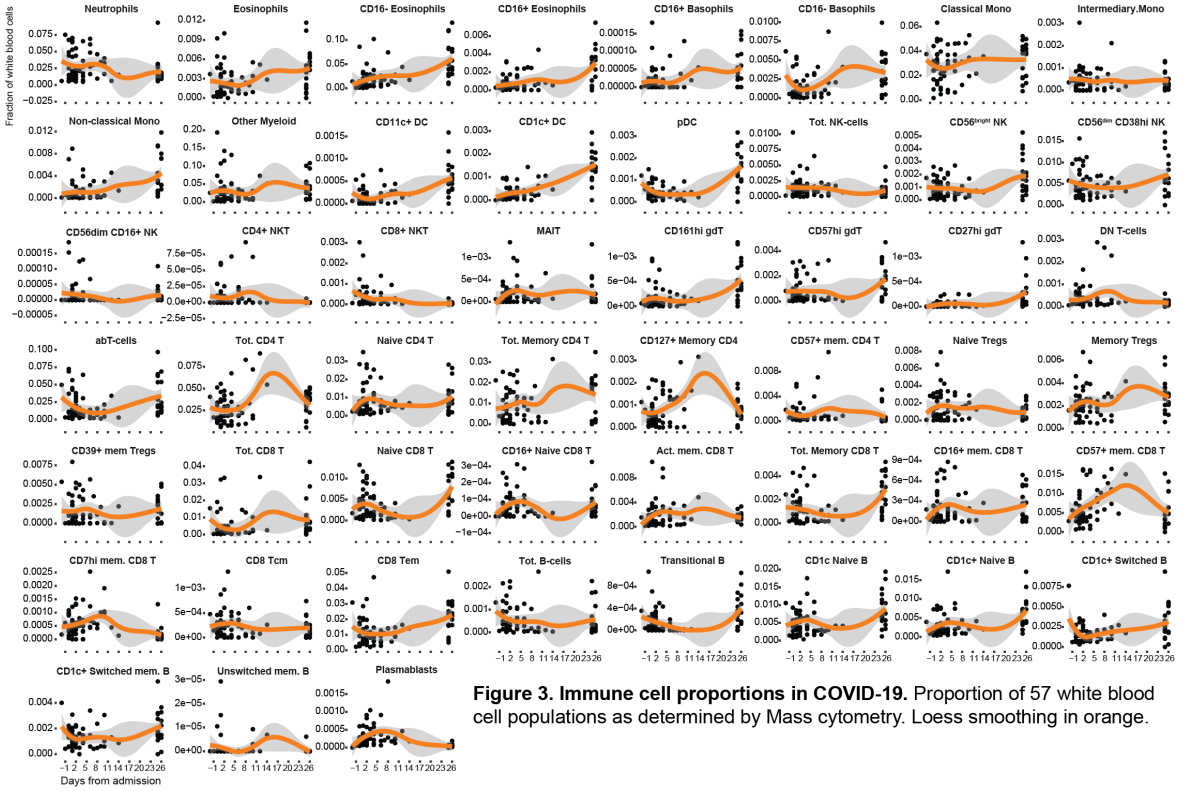

Figure 3. Immune cell proportions in COVID-19. Proportion of 57 white blood cell populations as determined by Mass cytometry. Loess smoothing in orange.

Eosinophil activation and homing during acute COVID-19

Given the changes in eosinophil abundance above, we decided to study Eosinophils more carefully. There are reports of strong GM-CSF responses in lungs of COVID-19 patients (Zhou et al., 2020) and GM-CSF is known to stimulate Eosinophils, particularly in interstitial pneumonia and allergic inflammation (Taniguchi et al., 2000). Taking advantage of the detailed longitudinal sample series, we used Partition-based graph abstraction, PAGA

(Wolf et al., 2019), to reconstruct single-cell phenotypic changes of blood eosinophils during acute COVID-19 (**Fig. 4**). Leiden clustering found 12 Eosinophils subsets and the main groups are annotated by defining features (**Fig. 4A)**. By splitting cells obtained from the different longitudinal samples, time-associated changes in eosinophil phenotypes are revealed with a transient expansion of CD62L^{+} Eosinphils from day 2 to day 6 after admission (**Fig. 4B)**. CD62L-upregulation on Eosinophils have been reported to be induced by IFNγ (Momose et al., 1999), one of the most elevated cytokines in severe COVID-19, and the IFNγ levels show a slight increase right around the same time as the expansion of CD62L+ Eosinophils (**Fig. 4C)**. This phenotype of Eosinophils is reminiscent of lung resident Eosinophils, rather than induced inflammatory eosinophils in circulation and such ung-homing cells have previously been reported as important homeostatic regulators of inflammatory responses in the lung (Mesnil et al., 2016) (**Fig. 4D**). It is tempting to think that this transient expansion of CD62L+ Eosinophils just prior to the time development of severe lung hyperinflamation around 1 week after admission is related to this immunopathology of the lungs in COVID-19 patients. To this end further investigation into this Eosinophil - IFNγ axis is required and might suggest novel therapies targeting this response to mitigate ARDS and lung inflammation.

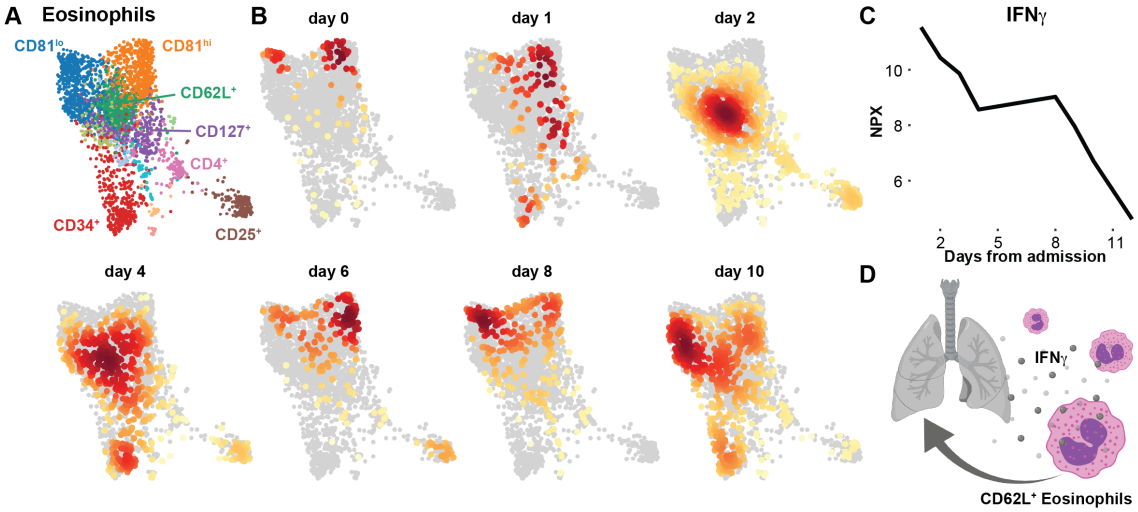

Figure 4. Eosinophil changes from admission to recovery. 2D representation generated by Partition-based graph abstraction (PAGA) of Eosinophils from patient COV-40 at 7 different timepoints from admission to recovery. (A) Louvain clusters are colored and annotated by key protein caracteristic and (B) cell distributions at each individual timepoint indicate changes in immune cell states and composition over time. (C) Plasma IFNγ levels as measured by Olink assay in plasma samples from the same patient COV-40. (**D**) IFNγ mediated upregulation of CD62L contributes to lung inflammation hyperinflammation.

211 **Adaptive immune cell dynamics during severe COVID-19**

212 Adaptive responses to SARS-CoV2 are seen in most individuals, with one study
213 reporting $CD4^+$ T-cell responses, and $CD8^+$ T-cell response in nearly all patients
214 (Grifoni et al., 2020). Similarly, the majority of symptomatic patients seroconvert
215 within a few days and most developed high-titer antibody responses (Sun et al.,
216 2020), yet one study has reported that a significant proportion of patients with
217 COVID-19 do not develop neutralizing antibody responses (Robbiani et al.,
218 2020). To investigate the dynamics of adaptive immune cell responses in our
219 cohort we used the same PAGA approach as described above. We find a clear
220 Plasmablasts response early after admission (**Fig. 5A**). The $CD4^+$ T-cell
221 response were initially dominated by effector and central memory responses,
222 followed by an increase in Tregs approximately four days after admission (**Fig.**
223 **5B**). The $CD4^+$ T-cells were split into two effector cell populations based CD4-
224 expression level, possible reflecting an activation-induced downregulation in a
225 subset of $CD4^+$ T-cells (**Fig. 5B**)(Grishkan et al., 2013). The $CD8^+$ T-cell
226 responses are dominated by activated cells expressing high CD38 and also a
227 subset of effector cells upregulating the CD147 receptor from about one week
228 onwards (**Fig. 5C**). Gamma-delta TCR T-cells, ($\gamma\delta$T-cells) and $CD8^+$ T-cells
229 progressively upregulated the marker of terminal maturation CD57 from about 1
230 week onwards (**Fig. 5C-D**). These results are largely in agreement with other
231 recent reports (Mathew et al., 2020) and highlight the strong innate and adaptive
232 immune activation during acute COVID-19.

233

234 **Cell-cell regulation varies over time during severe COVID-19**

235 Immune responses are always concerted efforts made by multiple, specialized
236 cell populations communicating via direct interactions and secreted cytokines
237 and other mediators. By studying such cell-cell relationships a better
238 understanding of the systems-level response can be obtained. We generated
239 cell-cell correlation matrices using longitudinal cell population frequencies and
240 binned the samples into four phases from acute disease to recovery phase (**Fig.**
241 **6A**). We find that the first phase (day 0-4) is dominated by an inverse correlation

242 between neutrophils and a number of myeloid and lymphoid cell types, as
243 reflected in the elevated NLR, associated with severe disease (Lagunas-Rangel,
244 2020)(**Fig. 6A**). The following phase (day 6-8) is characterized by a strong
245 coordinated Plasmablast, B-cell and $\alpha\beta$T-cell module, and this is inversely
246 correlated with a strong Treg and CD11c$^+$ DC module (**Fig. 6A**). From day 9
247 onwards a change is apparent with a shift towards a coregulated module
248 involving Eosinophils, pDCs, CD11c$^+$ DCs, with CD8$^+$ T-cells. This module is
249 largely maintained in the recovered patients, possibly reflecting a more normal
250 cell-cell relationship (**Fig. 6A**).
251
252 A prototype of a coordinated immune response to viruses is the appearance of
253 virus specific IgG antibodies because such responses elicited by B-cells require
254 help from CD4$^+$ T-cells. Here we investigated the seroconversion in this cohort
255 and found strong induction of IgG antibodies to the SARS-CoV2 Spike protein
256 (Receptor Binding Domain, RBD) in the majority of patients (**Fig. 6B**). This is in
257 line with similar analyses in other COVID-19 patients (Sun et al., 2020)(Amanat
258 et al., 2020). We were unable to test the neutralizing capacity of these antibodies
259 at this time, but another recent report has shown that a significant proportion of
260 patients mount antibodies that lack such neutralizing capacity (Robbiani et al.,
261 2020). To understand the immunological correlates of IgG responses to SARS-
262 CoV2, we devised a mixed effect model, using both plasma protein levels and
263 cell frequencies as predictors, taking days after admission into account as a fixed
264 effect (Chung et al., 2013). We found several features significantly associated
265 with IgG-responses, and in particular strong proinflammatory cytokines IFNγ, IL-
266 6, and chemokines CXCL10 and MCP-2 (CCL8) are negatively associated with
267 anti-CoV2 IgG responses (**Fig. 6C**). In contrast the Neutrophil-recruiting
268 chemokine CXCL6 are positively associated with anti-CoV2 IgG responses and
269 so was the fraction of circulating Basophils (**Fig. 6C**). It is known that basophils
270 are able to bind antigens on their surface and potentiate humoral immune
271 responses (Denzel et al., 2008) and since basophils are depleted during acute
272 and severe COVID-19 (**Fig. 3**), our data collectively suggest that the degree of

basophil depletion might influence the efficacy of IgG-responses to SARS-CoV2. It is believed that basophil mediated enhancement of B-cell responses occurs through the production of either IL-4 or IL-6, but levels of the latter were found to inversely associated with antibody responses (**Fig. 6C**) so it more likely that another mechanism is responsible for the basophil enhancement of IgG responses in the case of COVID-19. Collectively these results indicate a coordinate adaptive immune response to SARS-CoV2, enhanced by basophils and possibly suppressed by hyperinflammatory cytokine responses with high IL-6 levels during acute COVID-19.

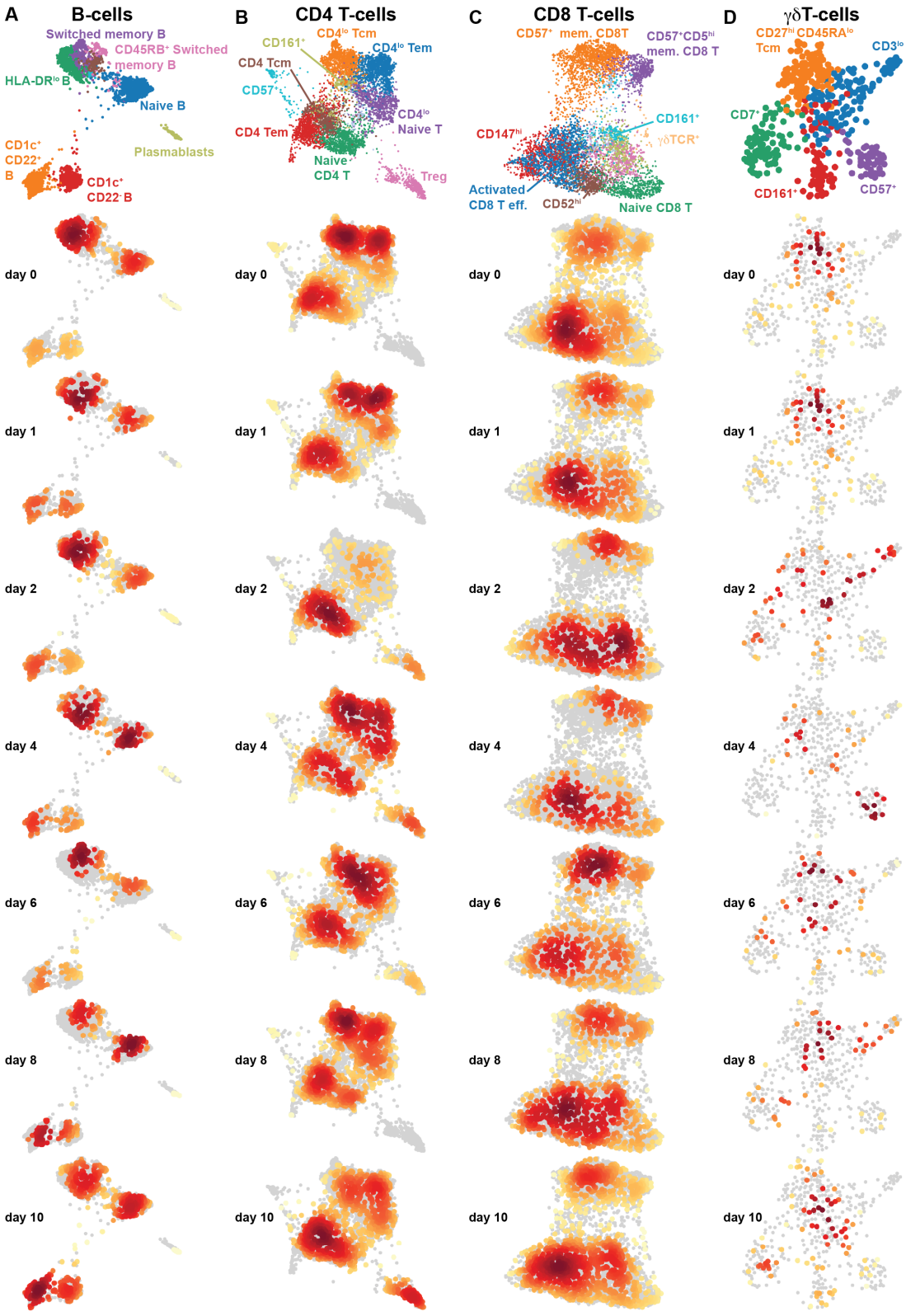

Figure 5. Adaptive immune cell changes from admission to recovery. (**A-D**) 2D representation generated by Partition-based graph abstraction (PAGA) B-cells, CD4 T-cells, CD8 T-cells and gdT-cells from patient COV-40 at 7 different timepoints from admission to recovery. Louvain clusters are colored (top) and annotated by key protein caracteristic and cell distributions at each individual timepoint indicate changes in immune cell states and composition over time.

A shared, integrated trajectory of recovery across patients

Since none of the patients in this cohort were treated with immunomodulatory agents, and have recovered with supportive care alone, we reasoned that a deeper investigation into the immunological changes during recovery from severe COVID-19 would be informative about the underlying immune processes involved. Given the strong interactions among immune cells and proteins in the immune system we applied an integrative analysis method to search for a multiomic trajectory of immune recovery. We used Multiomics Factor Analysis, MOFA (Argelaguet et al., 2018). This method allowed us to search for latent factors that best explain the variance across data types and use these to discern any possible relationship with the process of recovery from disease.

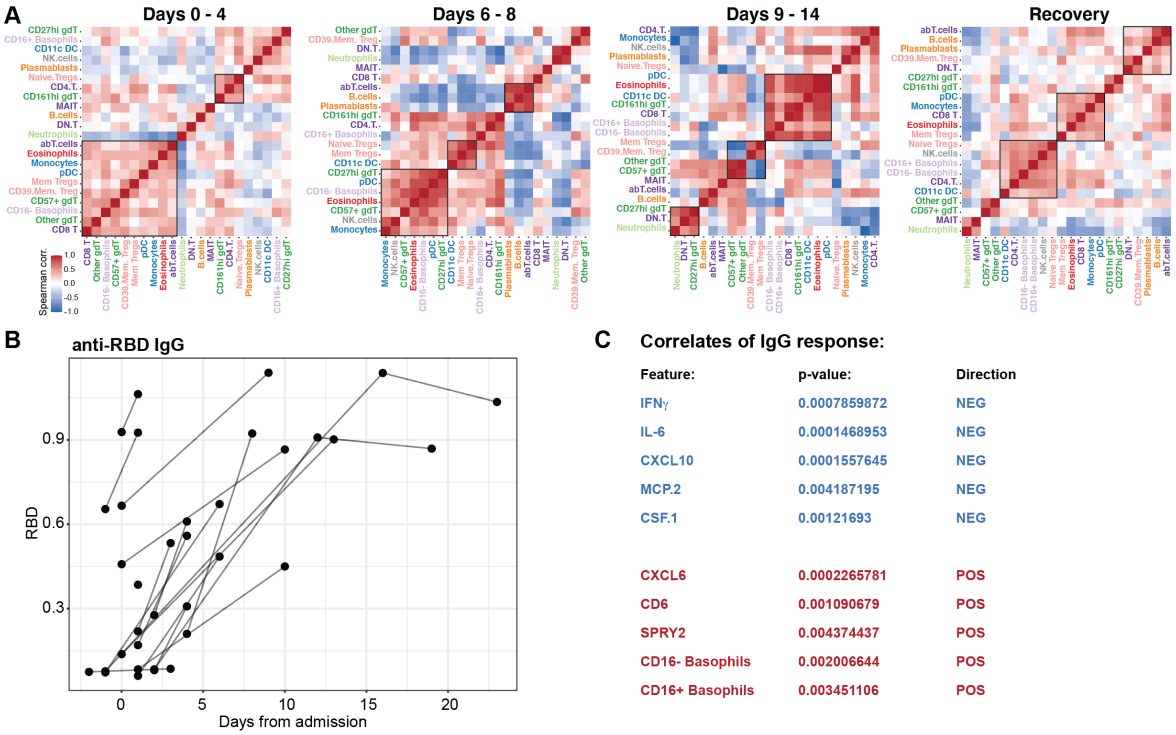

Figure 6. Cell-cell communications network during different phases from acute to recovery of COVID-19. (A) Spearman correlation matrices from samples collected at the indicated time intervals and ordered by top correlations. Co-regulated cell populations highlighted by boxes. (**B**) Serum IgG antibodies against SARS-CoV2 Spike protein Receptor Binding Domain, RBD shown against days after admission. (**C**) Mixed effect modeling, MEM of plasma protein levels and immune cell population frequencies against anti-RBD IgG titers. Five most positively and negatively associated features in MEM correlated with antibody responses when Days from admission is taking into account as a fixed effect.

We found ten latent factors that explained the variance in the combined dataset (**Fig. 7A**), and out of those, latent factor 2 was associated with the transition from acute to recovery phases of disease (**Fig. 7B**). There were no clear differences

among intensive care unit (ICU) or non-ICU ward patients and the levels of latent factor 2 were highest in the samples taken from recovered patients (**Fig. 7B**). To understand the biology of immune recovery we assessed the underlying features contributing to latent factor 2. The plasma proteins changing the most all decreased during recovery and most prominent were IL-6, MCP3, KRT19 (Keratin19), CXCL10, AREG and IFNγ (**Fig. 7C**). Conversely the cells that changed the most during recovery were classical and non-classical monocytes, $CD56^{dim}$ NK cells, Eosinophils and γδT-cells, all increasing in relative proportions during recovery (**Fig. 7D**). This shared, integrated trajectory reveal markers most indicative of recovery in patients with severe COVID-19 and if verified in independent sets of patients, these features could be valuable biomarkers to monitor during disease progression in order to detect a switch from acute to recovery phases in severe COVID-19.

In this manuscript we have performed an in depth, longitudinal analysis of the immune system in patients with severe COVID-19 during acute disease and until spontaneous recovery. The natural course of this process is mapped and found to be similar among patients. We find changes in cell populations, such as CD62L-expressing Eosinophils, triggered by IFNγ and likely contributing to hyperinflammation and ARDS during acute disease. We show that basophils are depleted during acute disease but recuperate during recovery and the levels of basophils are significantly correlated with the titers of IgG antibodies to SARS-CoV2 produced by B-cells. In contrast, high levels of IL-6 and IFNγ are negatively associated with humoral responses. Finally, we uncover an immunological trajectory of disease recovery shared among patients. These results can be useful for the development of better immunomodulatory strategies to mitigate hyperinflammatory responses, optimize antiviral IgG responses and monitoring of disease progression and recovery in patients with severe COVID-19.

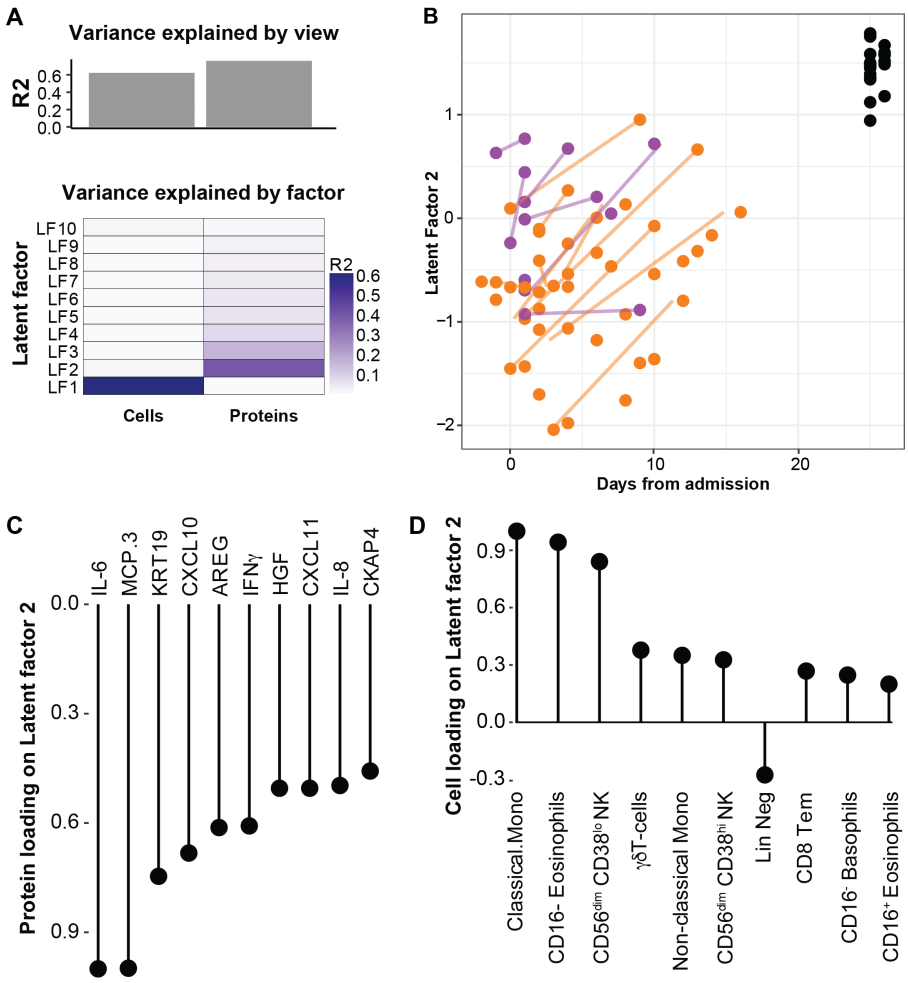

Figure 7. A multiomic immune signature from acute COVID-19 to recovery. Multiomics Factor Analysis, MOFA is used to integrate 148 plasma protein levels, and 63 immune cell frequencies across all 99 blood samples collected from 39 patients. (**A**) Fraction of total variance explained by type of measurement (view), and by Latent Factors, LFs 1-10. (**B**) LF2 best represent the changes from acute to recovery over time and reveal a shared trajectory for most patients. (**C**) Lollipop plot show plasma proteins explaining LF2. (**D**) Lollipop plot show cell populations explaining LF2.

DISCUSSION

A number of researchers are studying the immune response to SARS-CoV2 and we are learning that viral evasion of IFN-I/III signals and prevention of the normal induction Interferon-stimulated genes and the antiviral state (Blanco-Melo et al., n.d.). At the same time the proinflammatory response is strong. Secretion of chemokines and proinflammatory cytokines lead to influx of neutrophils and myeloid cells into the lung with strong local inflammatory responses and immunopathology (Vabret et al., 2020). Autopsy findings in patients succumbed to COVID-19 are characterized by perivascular T-cell infiltration, microangiopathy

339 and widespread thrombosis in the lung tissue (Ackermann et al., 2020). The
340 induction of IL-6 during severe COVID-19 have led to trials of blocking antibodies
341 to the IL-6 receptor with mixed results. This is inspired by Cytokine Release
342 Syndromes, CSR seen in cancer immunotherapy also often treated with IL-6
343 blocking agents. However, there are a number of differences between severe
344 COVID-19 and CRS, such as lower IL-6 levels, death caused by respiratory
345 failure and thrombosis, rather than from circulatory failure and status epilepticus
346 as seen in CRS (Vardhana and Wolchok, 2020). In this respect the mechanisms
347 of severe COVID-19 are incompletely understood and better understanding is
348 required for improved immunomodulatory therapies to be devised and
349 immunopathology and mortality limited.
350
351 Human immune systems are highly variable (Brodin and Davis, 2016), and most
352 of this variation is explained by environmental exposures (Brodin et al., 2015),
353 particularly early in life (Olin et al., 2018). The role of genetic variation in immune
354 variation in general and in COVID-19 in particular is under investigation
355 (Casanova et al., 2020). Systems-level analysis methods are useful in human
356 immunology because they capture the many variable cell populations, proteins
357 and transcriptional programs involved in a complex immune response. Systems-
358 level analyses also allow for the inference of relationships among such immune
359 system components (Lakshmikanth et al., 2020). In this study we add to the
360 rapidly growing literature by providing a longitudinal, systems-level perspective
361 on the immune system changes from acute to recovery phases of severe
362 COVID-19 disease. Longitudinal analyses are important because cross-sectional
363 analyses carry the risk of capturing snapshots of patients at different stages of
364 the immune response and thereby misinterpret differences as qualitatively
365 different. The longitudinal sampling presented herein is a strength of the current
366 study. Another important aspect of this work is its use of whole blood, rather than
367 peripheral blood mononuclear cells, allowing neutrophils, and other granulocyte
368 populations to be included in the analysis and also reduce the technical sources
369 of variation caused by cell preparation and freezing (Brodin et al., 2019). By

370 using this more holistic and longitudinal approach to analyze the immune
371 response during severe COVID-19, we find previously unappreciated roles of
372 Eosinophils in the acute response. These cells play important roles in other
373 respiratory infections (Flores-Torres et al., 2019) but have not been implicated
374 much in COVID-19. The population of eosinophils that expand a few days after
375 admission to the hospital were carachterized by CD62L-expression, a previously
376 reported marker of lung eosinophils (Mesnil et al., 2016) and it is probable that
377 this IFNγ-mediated upregulation of CD62L on eosinophils lead to the influx of
378 such cells into the lung tissue and the development of ARDS and clinical
379 deterioration often seen after about one week in many patients. The finding that
380 basophil levels are positively associated with humoral responses to SARS-CoV2
381 is intriguing and in line with previous studies in other viral infections (Denzel et
382 al., 2008). Further investigation will be required to understand the mechanisms
383 involved but it is likely not involving the production of IL-6 by basophils given that
384 plasma levels of this cytokine were inversely associated with IgG response titers
385 induced. Another possible mechanism involve IL-4 production by basophils,
386 known to potentiate B-cell responses to infection (Kawakami, 2008).
387
388 There has been a lot of concerns around antibody responses to SARS-CoV2 and
389 although nearly all patients with severe disease do produce antibodies in rather
390 high titers (Amanat et al., 2020; Grifoni et al., 2020), the neutralizing capability of
391 such antibodies are variable (Robbiani et al., 2020). One hypothesis brought
392 forward as a possible explanation to the severe disease occuring often after a
393 week or so of stable disease is antibody-mediated enhancement (ADE)(Iwasaki
394 and Yang, 2020; Tetro, 2020). This occurs when non-neutralizing antibodies bind a
395 virus and via Fc-receptors bring viruses into new cell types, not expressing the
396 receptor required forviral entry, in this case ACE2. Such reponses are well known
397 for Dengue virus infection and could induce hyperinflammatory responses also in
398 COVID-19. We have found that a significant proportion of $CD4^+$ T-cells in some
399 patients showed CD4 downregulation as a sign of possible cell activation, but
400 such downregulation can also occur if T-cells are directly infected (Xiang et al.,

401 2009). CD4$^+$ T-cells do not express ACE2 (Uhlen et al., 2019), but could express
402 Fc-receptors and therby be subject to viral infection and replication via ADE. This
403 is speculative at this time but as more data on determinants of neutralizing
404 antibody responses the theory of ADE as a cause of severe COVID-19 will be
405 testable and have important implications for vaccine development (Iwasaki and
406 Yang, 2020). The influence of basophils in modulating humoral responses to
407 SARS-CoV2 uncovered herein should also be taken into account as basophils
408 are depleted during acute disease and the severeity if such depletion might be an
409 important determinant of the antibody response to the virus.
410

411 **ACKNOWLEDGEMENTS**

412 The authors are grateful to private donations to Karolinska Institutet from Bure
413 Equity AB (Stockholm, Sweden) and Af Jochnick Foundation. The study was also
414 supported by grants from Academy of Finland to E.K. (308913) and S.H.
415 (323499) and Helsinki University Hospital (project M7100YLIT2) to P.P as well as
416 funding from Juho Vainio Foundation to O.V and A.K. We appreciate the hard
417 work of doctors and nurses at the Helsinki University Hospital.
418

419 **FIGURE LEGENDS**

420 **Figure 1. Longitudinal profiling of the immune system in moderate and**
421 **severe COVID-19.** (**A**) 180 unique plasma proteins were quantified using Olink
422 assays (n=77 plasma samples) and whole blood immune cells analyzed by Mass
423 cytometry (n=80 whole blood samples). (**B**) Monitoring and longitudinal sampling
424 of blood cells (X) and plasma (o) from 39 patients at the Helsinki University
425 Hospital.
426

427 **Figure 2. The natural course of severe COVID-19 from admission to clinical**
428 **recovery**. (**A**) Body temperature measurements from representative patients
429 over the course of 30 days from admission to the hospital in ICU and non-ICU
430 patients. (**B-C**) White blood cell counts, and Lymphocyte counts during acute and
431 recovery phase in COVID-19 patients. (**D-G**) Plasma levels of the indicated

432 proteins using Olink assays in longitudinal samples from acute patients (left) and
433 single measurements from recovered patients (right). NPX: Normalized Protein
434 expression.
435
436 **Figure 3. Immune cell proportions in COVID-19**. Proportion of 57 white blood
437 cell populations determined by mass cytometry. Loess smoothing in orange.
438
439 **Figure 4. Eosinophil changes from admission to recovery**. 2D representation
440 generated by Partition-based graph abstraction (PAGA) of Eosinophils from
441 patient COV-40 at 7 different timepoints from admission to recovery. (**A**) Louvain
442 clusters are colored and annotated by key protein characteristic and (**B**) cell
443 distributions at each individual timepoint indicate changes in immune cell states
444 and composition over time. (**C**) Plasma IFNγ levels as measured by Olink assay
445 in plasma samples from the same patient COV-40. (**D**) IFNγ mediated
446 upregulation of CD62L contributes to lung inflammation hyperinflammation.
447
448 **Figure 5. Adaptive immune cell changes from admission to recovery**. (**A-D**)
449 2D representation generated by Partition-based graph abstraction (PAGA) B-
450 cells, CD4 T-cells, CD8 T-cells and γδT-cells from patient COV-40 at 7 different
451 timepoints from admission to recovery. Louvain clusters are colored (top) and
452 annotated by key protein characteristic and cell distributions at each individual
453 time point indicate changes in immune cell states and composition over time.
454
455 **Figure 6. Cell-cell communications network during different phases from**
456 **acute to recovery of COVID-19**. (**A**) Spearman correlation matrices from
457 samples collected at the indicated time intervals and ordered by top correlations.
458 Co-regulated cell populations highlighted by boxes. (**B**) Serum IgG antibodies
459 against SARS-CoV2 Spike protein Receptor Binding Domain, RBD showed
460 against days after admission. (**C**) Mixed effect modelling, MEM of plasma protein
461 levels and immune cell population frequencies against anti-RBD IgG titers. Five
462 most positively and negatively associated features in MEM correlated with

463 antibody responses when Days from admission is taking into account as a fixed
464 effect.
465
466 **Figure 7. A multiomics immune signature from acute COVID-19 to recovery**.
467 Multiomics Factor Analysis, MOFA is used to integrate 148 plasma protein levels,
468 and 63 immune cell frequencies across all 99 blood samples collected from 39
469 patients. (**A**) Fraction of total variance explained by type of measurement (view),
470 and by Latent Factors, LFs 1-10. (**B**) LF2 best represent the changes from acute
471 to recovery over time and reveal a shared trajectory for most patients. (**C**)
472 Lollipop plot show plasma proteins explaining LF2. (**D**) Lollipop plot show cell
473 population frequencies explaining LF2.
474
475 **REFERENCES**

476 Ackermann, M., Verleden, S.E., Kuehnel, M., Haverich, A., Welte, T., Laenger,
477 F., Vanstapel, A., Werlein, C., Stark, H., Tzankov, A., et al. (2020). Pulmonary
478 Vascular Endothelialitis, Thrombosis, and Angiogenesis in Covid-19. New Engl J
479 Medicine.
480 Amanat, F., Stadlbauer, D., Strohmeier, S., Nguyen, T.H.O., Chromikova, V.,
481 McMahon, M., Jiang, K., Arunkumar, G.A., Jurczyszak, D., Polanco, J., et al.
482 (2020). A serological assay to detect SARS-CoV-2 seroconversion in humans.
483 Nat Med 1–4.
484 Argelaguet, R., Velten, B., Arnol, D., Dietrich, S., Zenz, T., Marioni, J.C.,
485 Buettner, F., Huber, W., and Stegle, O. (2018). Multi-Omics Factor Analysis—a
486 framework for unsupervised integration of multi-omics data sets. Mol Syst Biol
487 *14*, e8124.
488 Blanco-Melo, D., Nilsson-Payant, B.E., Liu, W.-C., Uhl, S., Hoagland, D., Møller,
489 R., Jordan, T.X., Oishi, K., Panis, M., Sachs, D., et al. (n.d.). Imbalanced host
490 response to SARS-CoV-2 drives development of COVID-19. Cell.
491 Brodin, P. (2018). The biology of the cell – insights from mass cytometry. Febs J.
492 Brodin, P. (2020). Why is COVID-19 so mild in children? Acta Paediatr.
493 Brodin, P., and Davis, M.M. (2016). Human immune system variation. Nat Rev
494 Immunol *17*, 21–29.
495 Brodin, P., Jojic, V., Gao, T., Bhattacharya, S., Angel, C.J.L., Furman, D., Shen-
496 Orr, S., Dekker, C.L., Swan, G.E., Butte, A.J., et al. (2015). Variation in the
497 Human Immune System Is Largely Driven by Non-Heritable Influences. Cell *160*,
498 37–47.
499 Brodin, P., Duffy, D., and Quintana-Murci, L. (2019). A Call for Blood—In Human
500 Immunology. Immunity *50*, 1335–1336.
501 Casanova, J.-L., Su, H.C., and Effort, C.H.G. (2020). A global effort to define the
502 human genetics of protective immunity to SARS-CoV-2 infection. Cell.

503 Chung, Y., Rabe-Hesketh, S., Dorie, V., Gelman, A., and Liu, J. (2013). A
504 Nondegenerate Penalized Likelihood Estimator for Variance Parameters in
505 Multilevel Models. Psychometrika *78*, 685–709.
506 Denzel, A., Maus, U.A., Gomez, M.R., Moll, C., Niedermeier, M., Winter, C.,
507 Maus, R., Hollingshead, S., Briles, D.E., Kunz-Schughart, L.A., et al. (2008).
508 Basophils enhance immunological memory responses. Nat Immunol *9*, 733–742.
509 Flores-Torres, A.S., Salinas-Carmona, M.C., Salinas, E., and Rosas-Taraco,
510 A.G. (2019). Eosinophils and Respiratory Viruses. Viral Immunol *32*, 198–207.
511 Grifoni, A., Weiskopf, D., Ramirez, S.I., Mateus, J., Dan, J.M., Moderbacher,
512 C.R., Rawlings, S.A., Sutherland, A., Premkumar, L., Jadi, R.S., et al. (2020).
513 Targets of T cell responses to SARS-CoV-2 coronavirus in humans with COVID-
514 19 disease and unexposed individuals. Cell.
515 Grishkan, I.V., Ntranos, A., Calabresi, P.A., and Gocke, A.R. (2013). Helper T
516 cells down-regulate CD4 expression upon chronic stimulation giving rise to
517 double-negative T cells. Cell Immunol *284*, 68–74.
518 Haveri, A., Smura, T., Kuivanen, S., Österlund, P., Hepojoki, J., Ikonen, N.,
519 Pitkäpaasi, M., Blomqvist, S., Rönkkö, E., Kantele, A., et al. (2020). Serological
520 and molecular findings during SARS-CoV-2 infection: the first case study in
521 Finland, January to February 2020. Eurosurveillance *25*, 2000266.
522 Huang, C., Wang, Y., Li, X., Ren, L., Zhao, J., Hu, Y., Zhang, L., Fan, G., Xu, J.,
523 Gu, X., et al. (2020). Clinical features of patients infected with 2019 novel
524 coronavirus in Wuhan, China. Lancet *395*, 497–506.
525 Iwasaki, A., and Yang, Y. (2020). The potential danger of suboptimal antibody
526 responses in COVID-19. Nat Rev Immunol 1–3.
527 Jacomy, M., Venturini, T., Heymann, S., and Bastian, M. (2014). ForceAtlas2, a
528 continuous graph layout algorithm for handy network visualization designed for
529 the Gephi software. Plos One *9*, e98679.
530 Jin, J.-M., Bai, P., He, W., Wu, F., Liu, X.-F., Han, D.-M., Liu, S., and Yang, J.-K.
531 (2020). Gender Differences in Patients With COVID-19: Focus on Severity and
532 Mortality. Frontiers Public Heal *8*, 152.
533 Kawakami, T. (2008). Basophils now enhance memory. Nat Immunol *9*, 720–
534 721.
535 Lagunas-Rangel, F.A. (2020). Neutrophil-to-lymphocyte ratio and lymphocyte-to-
536 C-reactive protein ratio in patients with severe coronavirus disease 2019
537 (COVID-19): A meta-analysis. J Med Virol.
538 Lakshmikanth, T., Muhammad, S.A., Olin, A., Chen, Y., Mikes, J., Fagerberg, L.,
539 Gummesson, A., Bergström, G., Uhlen, M., and Brodin, P. (2020). Human
540 immune system variation during one year. Biorxiv 2020.01.22.915025.
541 Lazear, H.M., Schoggins, J.W., and Diamond, M.S. (2019). Shared and Distinct
542 Functions of Type I and Type III Interferons. Immunity *50*, 907–923.
543 Lu, R., Zhao, X., Li, J., Niu, P., Yang, B., Wu, H., Wang, W., Song, H., Huang, B.,
544 Zhu, N., et al. (2020). Genomic characterisation and epidemiology of 2019 novel
545 coronavirus: implications for virus origins and receptor binding. Lancet *395*, 565–
546 574.
547 Lundberg, M., Eriksson, A., Tran, B., Assarsson, E., and Fredriksson, S. (2011).
548 Homogeneous antibody-based proximity extension assays provide sensitive and

549 specific detection of low-abundant proteins in human blood. Nucleic Acids Res
550 *39*, e102–e102.
551 Mathew, D., Giles, J.R., Baxter, A.E., Greenplate, A.R., Wu, J.E., Alanio, C.,
552 Oldridge, D.A., Kuri-Cervantes, L., Pampena, M.B., D'Andrea, K., et al. (2020).
553 Deep immune profiling of COVID-19 patients reveals patient heterogeneity and
554 distinct immunotypes with implications for therapeutic interventions. Biorxiv
555 2020.05.20.106401.
556 Medzhitov, R., and Janeway, C.A. (2002). Decoding the Patterns of Self and
557 Nonself by the Innate Immune System. Science *296*, 298–300.
558 Mesnil, C., Raulier, S., Paulissen, G., Xiao, X., Birrell, M.A., Pirottin, D., Janss,
559 T., Starkl, P., Ramery, E., Henket, M., et al. (2016). Lung-resident eosinophils
560 represent a distinct regulatory eosinophil subset. J Clin Investigation *126*, 3279–
561 3295.
562 Mikes, J., Olin, A., Lakshmikanth, T., Chen, Y., and Brodin, P. (2019). Mass
563 Cytometry, Methods and Protocols. Methods Mol Biology Clifton N J *1989*, 111–
564 123.
565 Momose, T., Okubo, Y., Horie, S., Takashi, S., Tsukadaira, A., Suzuki, J., Isobe,
566 M., and Sekiguchi, M. (1999). Interferon-γ Increases CD62L Expression on
567 Human Eosinophils. Int Arch Allergy Imm *120*, 30–33.
568 Olin, A., Henckel, E., Chen, Y., Lakshmikanth, T., Pou, C., Mikes, J., Gustafsson,
569 A., Bernhardsson, A.K., Zhang, C., Bohlin, K., et al. (2018). Stereotypic Immune
570 System Development in Newborn Children. Cell *174*, 1277-1292.e14.
571 Robbiani, D.F., Gaebler, C., Muecksch, F., Lorenzi, J.C.C., Wang, Z., Cho, A.,
572 Agudelo, M., Barnes, C.O., Gazumyan, A., Finkin, S., et al. (2020). Convergent
573 Antibody Responses to SARS-CoV-2 Infection in Convalescent Individuals.
574 Biorxiv 2020.05.13.092619.
575 Stadlbauer, D., Amanat, F., Chromikova, V., Jiang, K., Strohmeier, S.,
576 Arunkumar, G.A., Tan, J., Bhavsar, D., Capuano, C., Kirkpatrick, E., et al. (2020).
577 SARS-CoV-2 Seroconversion in Humans: A Detailed Protocol for a Serological
578 Assay, Antigen Production, and Test Setup. Curr Protoc Microbiol *57*, e100.
579 Sun, B., Feng, Y., Mo, X., Zheng, P., Wang, Q., Li, P., Peng, P., Liu, X., Chen,
580 Z., Huang, H., et al. (2020). Kinetics of SARS-CoV-2 specific IgM and IgG
581 responses in COVID-19 patients. Emerg Microbes Infec *9*, 940–948.
582 Taniguchi, H., Katoh, S., Kadota, J., Matsubara, Y., Fukushima, K., Mukae, H.,
583 Matsukura, S., and Kohno, S. (2000). Interleukin 5 and granulocyte-macrophage
584 colony-stimulating factor levels in bronchoalveolar lavage fluid in interstitial lung
585 disease. Eur Respir J *16*, 959–964.
586 Tetro, J.A. (2020). Is COVID-19 receiving ADE from other coronaviruses?
587 Microbes Infect *22*, 72–73.
588 Traag, V.A., Waltman, L., and Eck, N.J. van (2019). From Louvain to Leiden:
589 guaranteeing well-connected communities. Sci Rep-Uk *9*, 5233.
590 Uhlen, M., Karlsson, M.J., Zhong, W., Tebani, A., Pou, C., Mikes, J.,
591 Lakshmikanth, T., Forsström, B., Edfors, F., Odeberg, J., et al. (2019). A
592 genome-wide transcriptomic analysis of protein-coding genes in human blood
593 cells. Sci New York N Y *366*.

Vabret, N., Britton, G.J., Gruber, C., Hegde, S., Kim, J., Kuksin, M., Levantovsky, R., Malle, L., Moreira, A., Park, M.D., et al. (2020). Immunology of COVID-19: current state of the science. Immunity.
Vardhana, S.A., and Wolchok, J.D. (2020). The many faces of the anti-COVID immune response. J Exp Medicine *217*.
Wolf, F.A., Hamey, F.K., Plass, M., Solana, J., Dahlin, J.S., Göttgens, B., Rajewsky, N., Simon, L., and Theis, F.J. (2019). PAGA: graph abstraction reconciles clustering with trajectory inference through a topology preserving map of single cells. Genome Biol *20*, 59.
Xiang, J., McLinden, J.H., Rydze, R.A., Chang, Q., Kaufman, T.M., Klinzman, D., and Stapleton, J.T. (2009). Viruses within the Flaviviridae decrease CD4 expression and inhibit HIV replication in human CD4+ cells. J Immunol Baltim Md 1950 *183*, 7860–7869.
Zhou, Y., Fu, B., Zheng, X., Wang, D., Zhao, C., qi, Y., Sun, R., Tian, Z., Xu, X., and Wei, H. (2020). Aberrant pathogenic GM-CSF+ T cells and inflammatory CD14+CD16+ monocytes in severe pulmonary syndrome patients of a new coronavirus. Biorxiv 2020.02.12.945576.

CONTACT FOR REAGENT AND RESOURCE SHARING

All requests to: petter.brodin@ki.se

EXPERIMENTAL MODEL AND SUBJECT DETAILS

Non-interventional, observational study.

Ethics

The study was approved by the Ethics Committee of the Hospital District of Helsinki and Uusimaa (HUS/853/2020) and conducted in accordance with the Declaration of Helsinki. Written informed consent was obtained from all participants.

Patients

Inpatients

We included symptomatic patients with positive SARS-CoV-2 PCR test admitted to Helsinki University Hospital, Helsinki, Finland. Patients were recruited within five days after hospitalization. We excluded patients who had been considered by the attending clinician not to benefit from intensive care. We recruited 17 inpatients (9 females, 8 males) aged between 40 - 77 years. The duration of

631 hospitalization ranged from 5 to 38 days. Of these, 10 were admitted to the ICU,
632 and remained in intensive care for 1 - 27 days. Three patients required
633 mechanical ventilation for 3, 13 and 19 days, respectively.
634
635 *Recovery phase patients*
636 In addition to patients recruited during the acute phase of illness, we recruited a
637 separate cohort of recovered patients based on positive PCR (n=20) or high
638 clinical suspicion (n=2). These 22 subjects (age range 28 - 68 years; 11 females,
639 11 males) were included during convalescence 3-4 weeks after COVID-19
640 diagnosis and SARS-CoV-2 detection. These patients were identified from
641 medical and laboratory records, contacted by phone and invited to donate a
642 blood sample.
643
644 **METHOD DETAILS**
645 **Immunophenotyping by Mass Cytometry**
646 Blood samples drawn from patients with COVID-19 were mixed with a whole blood
647 stabilizer (Brodin et al., 2019)(Cytodelics AB, Sweden) either immediately or within
648 1-3 hrs post blood draw and cryopreserved as per the manufacturer's
649 recommendations. Samples were then thawed, and cells were fixed/RBCs lysed
650 using WASH # 1 and WASH # 2 buffers (Whole blood processing kit; Cytodelics
651 AB, Sweden) as per the manufacturer's recommendations. This was performed a
652 few days prior to barcoding and staining of cells. Post fix/lysis of cells, ~1-2x10^6
653 cells/sample were plated onto a 96 well round bottom plate using standard
654 cryoprotective solution (10% DMSO and 90% FBS) and cryopreserved at -80°C.
655
656 At the time of experimentation, cells were thawed at 37°C using RPMI medium
657 supplemented with 10% fetal bovine serum (FBS), 1% penicillin-streptomycin and
658 benzonase (Sigma-Aldrich, Sweden). Briefly, cells were barcoded using
659 automated liquid handling robotic system (Agilent technologies)(Mikes et al., 2019)
660 using the Cell-ID 20-plex Barcoding kit (Fluidigm Inc.) as per the manufacturer's
661 recommendations. Samples were pooled batch wise by keeping together the

662 longitudinal samples from each patient in the same batch. Cells were then washed,
663 FcR blocked using blocking buffer (in-house developed recipe) for 12 min at room
664 temperature, following which cells were incubated for another 30 min at 4°C after
665 addition of a cocktail of metal conjugated antibodies targeting the surface antigens.
666 Cells were washed twice with CyFACS buffer (PBS with 0.1% BSA, 0.05% sodium
667 azide and 2mM EDTA) and fixed overnight using 2% formaldehyde made in PBS
668 (VWR, Sweden). The broad extended panel of antibodies used are listed in
669 Supplementary Table 1. For acquisition by CyTOF, cells were stained with DNA
670 intercalator (0.125 µM Iridium-191/193 or MaxPar® Intercalator-Ir, Fluidigm) in 2%
671 formaldehyde made in PBS for 20 min at room temperature. Cells were washed
672 once with CyFACS buffer, PBS and milliQ water, and twice with Cell acquisition
673 solution (CAS) (Fluidigm). Cells were mixed with 0.1X Norm Beads (EQ™ Four
674 Element Calibration Beads, Fluidigm) filtered through a 35µm nylon mesh and
675 diluted to 1000,000 cells/ml. Cells were acquired using Helios mass cytometer at
676 a rate of 300-500 cells/s using PSI system, CyTOF software version 6.5.358 with
677 noise reduction, a lower convolution threshold of 400, event length limits of 10-150
678 pushes, a sigma value of 3, and flow rate of 0.030 ml/min.
679
680 **Antibodies and reagents**
681 Purified antibodies for mass cytometry were obtained in carrier/protein-free buffer
682 and then coupled to lanthanide metals using the MaxPar antibody conjugation kit
683 (Fluidigm Inc.) as per the manufacturer's recommendations. Following the protein
684 concentration determination by measurement of absorbance at 280 nm on a
685 nanodrop, the metal-labeled antibodies were diluted in Candor PBS Antibody
686 Stabilization solution (Candor Bioscience, Germany) for long-term storage at 4°C.
687 Antibodies used are listed in Supplementary Table 1.
688
689 **Plasma protein profiling**
690 Serum or plasma samples collected from patients with COVID-19 (by spinning
691 blood at 2000g for 10min at 80 C for plasma collection or by collecting serum from
692 those blood samples from which PBMCs were isolated using gradient

693 centrifugation for future use and not intended for this study) were analyzed using
694 a multiplex proximity extension assay (OLINK Bioscience, Uppsala, Sweden).
695 Each kit provides a microtiter plate for measuring 92 protein biomarkers. Two
696 panels, the Olink Immune Response and Inflammation panels. Each well contains
697 96 pairs of DNA-labeled antibody probes. Samples were incubated in the presence
698 of proximity antibody pairs tagged with DNA reporter molecules. When the
699 antibody pair bounds to their corresponding antigens, the corresponding DNA tails
700 form an amplicon by proximity extension, which can be quantified by high-
701 throughput real-time PCR.
702
703 **Detection of anti-SARS-CoV-2 antibody response**
704 Antibodies against SARS-CoV-2 were measured using indirect
705 immunofluorescence assay (IFA) and enzyme-linked immunosorbent assay
706 (ELISA) using SARS-CoV-2 receptor-binding domain (RBD) as the antigen. The
707 IFA was conducted as described (Haveri et al., 2020). The RBD ELISA was done
708 following a recently published protocol (Amanat et al., 2020; Stadlbauer et al., 2020).
709 The RBD antigen was produced by transient transfection of RBD plasmid to Vero
710 E6 cells and the produced protein was purified following established protocol
711 (Stadlbauer et al., 2020). The raw data is available in Supplementary Table 2.
712
713 **QUANTIFICATION AND STATISTICAL ANALYSIS**
714 **Mass Cytometry Preprocessing and Gating**
715 All FCS-files unrandomized using the CyTOF software (version 6.0.626) were
716 transferred without any additional preprocessing.
717
718 **Multiomics Factor Analysis, MOFA**
719 MOFA (Argelaguet et al., 2018) uses a set of data matrices as input, plasma protein
720 expression and cell abundance datasets were used to build the *MOFAobject* with
721 *MultiAssayExperiment*. The MOFA object was trained in R through the *reticulate*
722 package with 10 factors and a variance threshold of 0.01%. Both omics datasets
723 were processed individually to remove any features resulting in zero or low

variance before fitting the model. Convergence of the model was assessed using the change in ELBO (deltaELBO) to verify it fit the convergence threshold which is considered to be between 1 and 10. Multiple models were run under different initializations to validate that factors were consistent across trials for model selection.

Partition-based graph abstraction of single-cell data

The CyTOF data were first preprocessed with arcsin h and scaled to unit variance and then partitioned into different subpopulations according to our in-house supervised learning algorithm. For each subpopulation, the phenotypic changes over different time points are inferred with a trajectory inference method called PAGA (Wolf et al., 2019). In brief, PCA was first applied to reduce the number of features to 20, and then the clusters were detected with Leiden method (Traag et al., 2019). Afterwards, the Leiden output was used by PAGA to infer a trajectory map of clusters. Finally, the PAGA graph was taken as the initial position by ForceAtlas2 (FA)(Jacomy et al., 2014) for the single-cell level visualization.

Mixed effects modeling

A partially Bayesian method was applied with *blme* package on both datasets (plasma protein expression and cell abundance) to produce maximum a posteriori (MAP) estimates (Chung et al., 2013). This provided the ability to nest the variables, and account for days from admission as well as RBD levels.

DATA AND SOFTWARE AVAILABILITY

Raw Mass cytometry data is available for download:

https://ki.box.com/s/sby0jesyu23a65cbgv51vpbzqjdmipr1

755

756 **Suppl. Table 1. Antibodies used for Mass cytometry.**

Metal tag	Marker	Clone	Vendor
89Y	CD45	HI30	Fluidigm
110Cd	CD33	WM53	Biolegend
111Cd	CD26	BA5b	Biolegend
112Cd	CD11c	Bu15	Biolegend
113Cd	IgD	IA6-2	Biolegend
114Cd	HLA-DR	L243	BioLegend
115In	CD57	HCD57	Biolegend
141Pr	CD49d	9F10	Fluidigm
142Nd	CD43	84-3C1	eBiosciences
143Nd	CD3e	UCHT1	Biolegend
144Nd	CD45RB	MEM-55	Biolegend
145Nd	CD81	5A6	Biolegend
146Nd	CD52	HI186	Biolegend
147Sm	CD1c	L161	Biolegend
148Nd	CD55	JS11	Biolegend
149Sm	CD25	2A3	Fluidigm
150Nd	CD64	10.1	Biolegend
151Eu	CD123	6H6	BioLegend
152Sm	TCRgd	5A6.E9	Fischer Scientific
153Eu	Siglec-8	837535	R&D Systems
154Sm	CD95	DX2	BioLegend
155Gd	CX3CR1	8E10.D9	BioLegend
156Gd	CD20	2H7	BioLegend
157Gd	CD9	SN4 C3-3A2	eBiosciences
158Gd	CD34	581	Biolegend
159Tb	CD22	HIB22	Biolegend
160Gd	CD14	M5E2	Biolegend
161Dy	CD161	HP-3G10	Biolegend
162Dy	CD29	TS2/16	Biolegend
163Dy	4-1BB	4B4-1	Biolegend
164Dy	CD62L	DREG-56	Biolegend
165Ho	CD127	A019D5	Fluidigm
166Er	CD24	ML5	Biolegend
167Er	CD27	L128	Biolegend

168Er	CD141	M80	Biolegend
169Tm	CD45RA	HI100	Fluidigm
170Er	CD38	HIT2	Biolegend
171Yb	CD85j	GHI/75	Biolegend
172Yb	CD147	HIM6	BioLegend
173Yb	CD56	NCAM16.2	BD Pharmingen
174Yb	CD99	HCD99	Biolegend
175Lu	CD28	CD28.2	Biolegend
176Yb	CD39	A1	Biolegend
191Ir	DNA Ir	Cell-ID DNA Intercalator	Fluidigm
193Ir	DNA Ir	Cell-ID DNA Intercalator	Fluidigm
194Pt	CD8a	SK1	BD Pharmingen
195Pt	CD5	UCHT2	Biolegend
196Pt	CD7	CD7-6B7	Biolegend
198Pt	CD4	RPA-T4	Biolegend
209Bi	CD16	3G8	Fluidigm

757

758 **Suppl. Table 2. IgG data**

Sample ID	Subject ID	IFA (inf. cells)	old-RBD	VE6-RBD
CoV-24, seerumi 12.4.20	COV-24	320	0.138	0.064
CoV-24, heparin 24.4.20	COV-24	2570	0.902	0.2025
CoV-25, seerumi 12.4.20	COV-25	320	0.219	0.0795
CoV-25, EDTA 14.4.20	COV-25	1280	0.533	0.118
CoV-26, seerumi 14.4.20	COV-26	2560	0.458	0.1015
CoV-26, heparin 24.4.20	COV-26	2570	0.866	0.163
CoV-27, seerumi, 15.4.20	COV-27	640	0.666	0.1415
CoV-27, heparin, 24.4.20	COV-27	1280	1.139	0.218
CoV-28, seerumi, 18.4.20	COV-28	640	0.385	0.1
CoV-29, seerumi, 20.4.20	COV-29	160	0.21	0.085
CoV-29, heparin, 24.4.20	COV-29	1280	0.923	0.1865
CoV-30, seerumi, 20.4.20	COV-30	1280	0.928	0.1895
CoV-30, seerumi, 22.4.20	COV-30	2570	1.063	0.215
CoV-31, seerumi, 20.4.20	COV-31	320	0.654	0.135
CoV-31, seerumi, 22.4.20	COV-31	640	0.926	0.185
CoV-32, seerumi, 21.4.20	COV-32	80	0.084	0.0645
CoV-32, heparin, 30.4.20	COV-32	1280	0.45	0.1035

CoV-33, seerumi, 21.4.20	COV-33	80	0.17	0.0685
CoV-33, heparin, 24.4.20	COV-33	640	0.559	0.112
CoV-34, EDTA, 21.4.20	COV-34	10	0.077	0.0625
CoV-34, EDTA, 8.5.20	COV-34	2560	1.138	0.267
CoV-34, EDTA, 15.5.20	COV-34	2560	1.035	0.237
CoV-35, seerumi, 23.4.20	COV-35	10	0.073	0.06
CoV-35, heparin, 30.4.20	COV-35	2560	0.672	0.141
CoV-36, seerumin, 22.4.20	COV-36	10	0.061	0.057
CoV-36, seerumi, 27.4.20	COV-36	640	0.485	0.117
CoV-37, seerumi, 22.4.20	COV-37	10	0.075	0.0615
CoV-37, heparin, 27.4.20	COV-37	80	0.086	0.063
CoV-39, seerumi, 28.4.20	COV-39	640	0.277	0.081
CoV-39, heparin, 30.4.20	COV-39	640	0.61	0.123
CoV-40, seerumi, 28.4.20	COV-40	1280	0.084	0.065
CoV-40, heparin, 8.5.20	COV-40	2570	0.909	0.2445
CoV-40, EDTA, 15.5.20	COV-40	2560	0.869	0.216
CoV-41, seerumi, 28.4.20	COV-41	320	0.081	0.0615
CoV-41, heparin, 30.4.20	COV-41	640	0.308	0.0985

759

760 **Suppl. Table 3. Raw Olink data**

761